Determinants of the Rate of mRNA Translocation in Bacterial Protein Synthesis

Anneli Borg[1,2] and Måns Ehrenberg[1]

1 - Department of Cell and Molecular Biology, Biomedical Center, Uppsala University, Box 596, 751 24 Uppsala, Sweden
2 - 3H Biomedical AB, Dag Hammarskjölds väg 34A, Uppsala Science Park, 751 83 Uppsala, Sweden

Correspondence to Måns Ehrenberg: ehrenberg@xray.bmc.uu.se
http://dx.doi.org/10.1016/j.jmb.2014.10.027
Edited by R. L. Gonzalez

Abstract

Studying the kinetics of translocation of mRNA and tRNAs on the translating ribosome is technically difficult since the rate-limiting steps involve large conformational changes without covalent bond formation or disruption. Here, we have developed a unique assay system for precise estimation of the full translocation cycle time at any position in any type of open reading frame (ORF). Using a buffer system optimized for high accuracy of tRNA selection together with high concentration of elongation factor G, we obtained *in vivo* compatible translocation rates. We found that translocation was comparatively slow early in the ORF and faster further downstream of the initiation codon. The maximal translocation rate decreased from the *in vivo* compatible value of 30 s^{-1} at 1 mM free Mg^{2+} concentration to the detrimentally low value of 1 s^{-1} at 6 mM free Mg^{2+} concentration. Thus, high and *in vivo* compatible accuracy of codon translation, as well as high and *in vivo* compatible translocation rate, required a remarkably low Mg^{2+} concentration. Finally, we found that the rate of translocation deep inside an ORF was not significantly affected upon variation of the standard free energy of interaction between a 6-nt upstream Shine-Dalgarno (SD)-like sequence and the anti-SD sequence of 16S rRNA in a range of 0–6 kcal/mol. Based on these experiments, we discuss the optimal choice of Mg^{2+} concentration for maximal fitness of the living cell by taking its effects on the accuracy of translation, the peptide bond formation rate and the translocation rate into account.

Introduction

Estimates of the average rate of peptide elongation in the living *Escherichia coli* cell display weak growth rate dependence and are normally confined to a range of 14- to 22-amino-acid incorporations per ribosome per second [1–3]. A peptide elongation cycle includes the time for binding of aminoacyl-tRNA in ternary complex with elongation factor Tu (EF-Tu) and GTP to the ribosomal A site, GTP hydrolysis on EF-Tu, release of EF-Tu in the GDP form from the ribosome, peptidyl transfer, binding of elongation factor G (EF-G) in the GTP form to the ribosome, GTP hydrolysis on EF-G, translocation of the mRNA and the tRNAs and release of EF-G in the GDP form from the ribosome (see Schmeing and Ramakrishnan [4] for a review). To be compatible with *in vivo* experiments, all these steps must be completed within 50–70 ms. It is, however, possible that the average rate of the peptide elongation cycle

is even faster since rate estimates based on the cellular ribosome concentration and ribosome elongation activity often depend on the assumption that protein degradation is negligible during growth of bacteria in early logarithmic phase [3,5]. If proteins are degraded to a significant extent [6–8], the time for the multistep peptide elongation cycle would be even shorter.

Compared to the peptide bond formation process, which includes tRNA binding to the ribosome, tRNA accommodation in the A site and peptidyl transfer, the rates of major steps of the translocation process have received little attention. Translocation involves one covalent change, the very rapid hydrolysis of GTP on EF-G just after association of the factor to the pre-translocation ribosome [9]. It is, according to the current understanding, only after GTP hydrolysis that the intricate dynamics of translocation takes place [9]. This includes the movement of the mRNA by one codon relative to the ribosomal frame and

shifting of the peptidyl-tRNA in the A/P site and the deacylated tRNA in the P/E site to the P/P and the E/E sites, respectively. These movements are accompanied by back-ratcheting of the ribosome from a state in which the ribosomal subunits are rotated in relation to each other to the non-ratcheted state of the post-translocation ribosome [10]. These steps occur without covalent changes, which has rendered their resolution and interpretation difficult. However, recent progress has been made by application of fluorescence techniques, in which ribosomes, mRNAs or tRNAs have been labeled with fluorophores, to detect conformational changes with classical stopped-flow [11–13] and single-molecule techniques [14]. Furthermore, labeling of the 3′-end of mRNAs has made it possible to directly monitor their movement in relation to the ribosomal frame [11], and the release of phosphate from EF-G after GTP hydrolysis has been monitored by stopped-flow techniques [15,16]. The relative ratcheting movement of ribosomal subunits has been studied by Förster resonance energy transfer techniques in classical [12] and single-molecule [14,17] experiments. Single-molecule experiments are, however, often characterized by low elongation factor concentrations, yielding low peptide elongation rates.

A dramatic trade-off between the rate of amino acid incorporation and the accuracy of codon selection by tRNAs has been demonstrated [18]. It was found by variation of the Mg^{2+} concentration that the efficiency of association (k_{cat}/K_m) of cognate ternary complex to mRNA-programmed ribosomes decreased linearly with increasing accuracy of codon selection. This suggests that there exists an Mg^{2+} concentration optimal for maximal growth rate at which the negative effect of reduced kinetic efficiency of the ribosome is exactly compensated for by the positive effect of increased accuracy of codon reading [19]. To identify the optimal ionic composition for maximal ribosome efficiency, it is, however, necessary to consider also other aspects of ribosome function and, in particular, how the rate of translocation responds to an altered Mg^{2+} concentration. Fluorescence experiments, in which the movement of the mRNA on the translocating ribosome was monitored, have been carried out at different concentrations of Mg^{2+} ions [20]. It was found that decreasing Mg^{2+} concentration led to increasing rate of mRNA movement, but the experiment contained no information about subsequent steps, like back-ratcheting of the ribosome and EF-G release.

It follows from the law of mass action that the time of ternary complex binding to the ribosome decreases with increasing ternary complex concentration. From such considerations, it has been proposed that codons read by tRNAs of low abundance are translated more slowly than those read by high abundance tRNAs [21] and that this feature is used

by cells to optimize co-translational protein folding [22]. In contrast, recent observations based on ribosome profiling with deep sequencing suggested that the elongation rate is virtually independent of tRNA abundance in both bacteria and eukaryotes [23–25]. Furthermore, the only statistically significant cause of codon-specific variation of the protein elongation rate was due to variations in the free energy of interaction between Shine-Dalgarno (SD)-like sequences in open reading frames (ORFs) of translated mRNAs and the anti-SD sequence of 16S rRNA [26]. This is in line with the previous observation that internal SD sequences promote translational frameshifting and more recent single-molecule experiments showing that elongation is slowed down downstream of SD-like sequences [27].

These examples may serve to highlight the urgent need to improve the *in vitro* biochemistry to assess the time of the full translocation cycle during synthesis of short peptides and full-length proteins under *in vivo*-like conditions. Here, we have developed a biochemical system to monitor single translocation cycles in all types of ORFs. In this assay system, we measure the complete translocation cycle time from the association of EF-G·GTP to the pre-translocation ribosome to the release of EF-G·GDP from the post-translocation ribosome. This approach contrasts those based on fluorescence-labeled mRNA, fluorescence-labeled tRNAs or those with puromycin reactivity as a marker for the post-termination ribosomal complex (see Holtkamp *et al.* [28]). The method has been used to determine how the Mg^{2+} ion concentration affects the rate of translocation at high and low concentration of EF-G, how the rate of translocation varies with the distance between the translocated codon and the initiation codon and how SD-like sequences within ORFs affect the translocation rate. With support from these observations, we discuss mechanistic aspects of translocation, optimal conditions for maximal growth rate and fitness and further experiments to characterize the tuning of the protein elongation rate by internal SD–anti-SD interactions in the living cell.

Results

Translocation rates in different ORFs: Experimental method

Each peptide elongation cycle has two major phases. The first is the process of peptide bond formation. It includes aminoacyl-tRNA binding to the ribosome in ternary complex with EF-Tu·GTP, GTP hydrolysis on EF-Tu, tRNA accommodation in the ribosomal A site and peptidyl transfer. Its end-state is a ribosome with an A-site-bound peptidyl-tRNA and a P-site-bound deacylated tRNA. For convenience, this process is below denoted as "peptide bond formation". The second phase is the translocation

process. It includes binding of EF-G in the GTP form to the pre-translocation ribosome, GTP hydrolysis, translocation of mRNA and tRNAs and dissociation of EF-G in the GDP form. Its end-state is a ribosome with a P-site-bound peptidyl-tRNA. After EF-G dissociation from the ribosome, the A site is empty and ready to accept another ternary complex at the beginning of the next peptide elongation cycle (Fig. 1a).

To estimate the complete translocation time, τ_{trans}, from binding of EF-G·GTP to the pre-translocation ribosome to dissociation of EF-G·GDP from the post-translocation ribosome, we estimated the total time, τ_{tot}, to make a peptide bond at a selected codon in

an ORF, to translocate the mRNA and to make a second peptide bond at the subsequent codon. We also estimated the time for the first, τ_{p1}, and the second, τ_{p2}, peptide bond formation events and obtained τ_{trans} by subtracting the peptide bond formation times from the total time: $\tau_{trans} = \tau_{tot} - \tau_{p1} - \tau_{p2}$ (see Fig. 1a). To illustrate the principle of such measurements, we used ribosomes programmed with an mRNA template encoding the peptide fMH$_6$A$_6$LYF (see sequence in Fig. 2c). To estimate τ_{tot}, we rapidly mixed ribosome complexes with fMH$_6$A$_6$[^{14}C]L-tRNA^{Leu} in the P site, a Tyr codon in the A site and an adjacent, downstream Phe codon (complex A in Fig. 1a), with a factor mixture
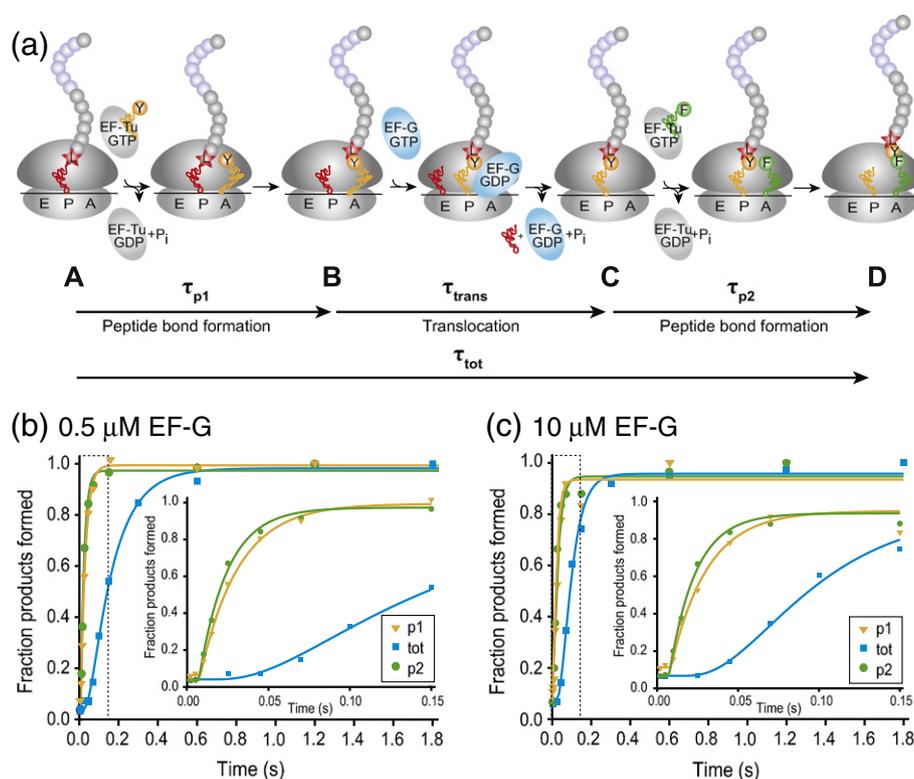

Fig. 1. The principle for determination of the translocation time. (a) Schematic representation of two subsequent peptide bond formation steps and the intervening translocation step of which the translocation time (τ_{trans}) was to be determined. τ_{tot}, τ_{p1} and τ_{p2} were determined in three parallel reactions, and from these, the translocation time was estimated as $\tau_{trans} = \tau_{tot} - \tau_{p1} - \tau_{p2}$. In the first reaction, complex A was rapidly mixed in a quench-flow instrument with EF-G and ternary complexes with unlabeled Tyr-tRNA^{Tyr} and [^{3}H]Phe-tRNA^{Phe}. The emergence of complex D was followed and gave the total time (τ_{tot}) for formation of the first peptide bond, translocation and formation of the second peptide bond. In a second reaction, complex A was mixed with EF-G and ternary complexes with [^{3}H]Tyr-tRNA^{Tyr} and unlabeled Phe-tRNA^{Phe}. The emergence of complex B gave the time for the first peptide bond formation (τ_{p1}). In a third reaction, complex C was mixed with EF-G and ternary complexes with unlabeled Tyr-tRNA^{Tyr} and [^{3}H]Phe-tRNA^{Phe}. The emergence of complex D gave the time of the second peptide bond formation (τ_{p2}). (b) Time courses of the reactions described in (a) obtained at 0.5 μM EF-G concentration and ternary complex concentrations of 1.5 μM each. The time course of the overall three-step reaction (blue trace) and of the first (orange trace) and second (green trace) peptide bond formations were fitted to the three-step model described in (a). The translocation time (τ_{trans}) was 124 ± 8 ms and the two peptide bond formation times were 32 ± 2 ms (τ_{p1}) and 25 ± 1 ms (τ_{p2}). The inset shows the first 150 ms of the reaction in magnification, as indicated by the broken line. (c) Time courses for a translocation experiment obtained at 10 μM EF-G and ternary complex concentrations of 1.5 μM. The translocation time (τ_{trans}) was 51 ± 8 ms and the two peptide bond formation times were 31 ± 4 ms (τ_{p1}) and 24 ± 3 ms (τ_{p2}). The inset shows the first 150 ms of the reaction in magnification, as indicated by the broken line.
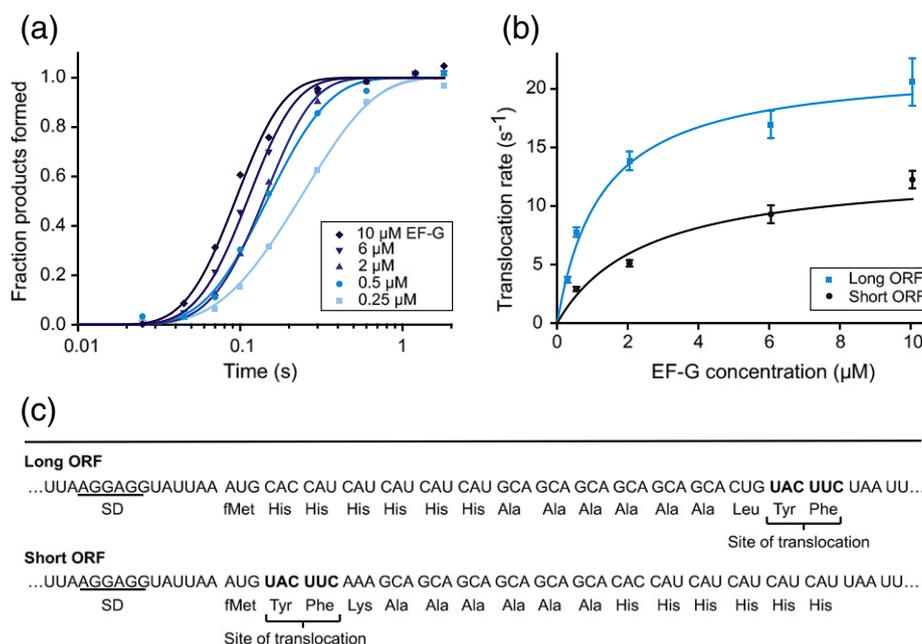
Fig. 2. Translocation rate dependency on EF-G concentration in a long ORF and a short ORF. (a) Time courses for the three-step process of peptide bond formation, translocation and a second peptide bond formation at 0.25–10 µM EF-G and 1.5 µM ternary complex concentrations in the long ORF. Peptide bond formation rates were determined in parallel experiments at each EF-G concentration and did not vary with the EF-G concentration (data not shown). (b) Comparison of EF-G concentration dependence in the long (blue trace) and the short (black trace) ORFs. The translocation rate was plotted against the EF-G concentration and fitting of the data to the Michaelis–Menten equation gave $k_{cat} = 22 \pm 3$ s^{-1} and $K_M = 1.3 \pm 0.3$ µM for the long ORF and $k_{cat} = 13 \pm 4$ s^{-1} and $K_M = 2.5 \pm 1.3$ µM for the short ORF. (c) Nucleotide and peptide sequences of the long and the short ORF template (the SD sequence is underlined). The site at which the translocation rate was determined is indicated for both templates.

in a quench-flow instrument. The factor mixture contained EF-G and ternary complexes with unlabeled Tyr-tRNA^{Tyr} and radiolabeled [^{3}H]Phe-tRNA^{Phe}. After mixing, fMH$_6$A$_6$[^{14}C]LY-tRNA^{Tyr} was rapidly formed in the A site (complex B in Fig. 1a) and translocated into the P site (complex C in Fig. 1a). Then, fMH$_6$A$_6$[^{14}C]LY was transferred to [^{3}H]Phe-tRNA^{Phe} in the A site by formation of fMH$_6$A$_6$[^{14}C]LY[^{3}H]Phe-tRNA^{Phe} (complex D in Fig. 1a). The time-dependent formation of complex D is shown in Fig. 1b (blue trace). In a parallel experiment to measure τ_{p1}, complex A was mixed with a factor mixture containing EF-G and ternary complexes with [^{3}H]Tyr-tRNA^{Tyr} and unlabeled Phe-tRNA^{Phe}, leading to rapid formation of fMH$_6$A$_6$[^{14}C]L[^{3}H]Tyr-tRNA^{Tyr} (complex B) and translocation followed by rapid formation of fMH$_6$A$_6$[^{14}C]L[^{3}H]TyrPhe-tRNA^{Phe} (complex D). The time-dependent incorporation of [^{3}H]Tyr into nascent peptide is shown in Fig. 1b (orange trace). In a parallel experiment to measure τ_{p2}, preformed complex C was mixed with a factor mixture containing EF-G and ternary complexes with [^{3}H]Phe-tRNA^{Phe} and unlabeled Tyr-tRNA^{Tyr}. EF-G and unlabeled Tyr-tRNA^{Tyr} were added to make the reaction conditions equal in the three types of experiments. This reaction led to rapid formation of

fMH$_6$A$_6$[^{14}C]LTyr[^{3}H]Phe-tRNA^{Phe} (complex D), and the time-dependent incorporation of [^{3}H]Phe into peptide is shown in Fig. 1b (green trace). All His-tagged peptides (fMH$_6$A$_6$LYF) were purified by nickel-affinity chromatography and their ^{14}C and ^{3}H contents quantified by scintillation counting. To minimize the effect of varying peptide recovery, we normalized the ^{3}H contents to the ^{14}C-Leu content of the samples. This internal standard procedure contributed greatly to the precision of the translocation time estimates, assessed as previously described (Materials and Methods and Johansson *et al.* [29]). The precision of the time estimates was further increased by joint fitting of the experimentally measured conversion of complex A via complex B and complex C to complex D to a kinetic model with three irreversible steps with the average times τ_{p1}, τ_{p2} and τ_{trans}. Figure 1b illustrates a translocation experiment at low (0.5 µM) EF-G concentration and with each ternary complex at 1.5 µM. The translocation time, τ_{trans}, was 124 ± 8 ms and the two peptide bond formation times, τ_{p1} and τ_{p2}, were 32 ± 2 ms and 25 ± 1 ms, respectively. Figure 1c illustrates an experiment with high (10 µM) EF-G concentration and with each ternary complex at 1.5 µM concentration. In this experiment, the translocation time, τ_{trans},

was 51 ±8 ms and the two peptide bond formation times, τ_{p1} and τ_{p2}, were 31 ± 4 ms and 24 ± 3 ms, respectively. The method described here can be applied to translocation time measurements in all types of ORFs encoding a His-tag upstream of the translocation step of study, but His-tag-lacking small peptides must be purified by other means, for example, by HPLC techniques with online radiometry, as described in the next section.

Translocation rate variation with free EF-G concentration

Here, we used the same experimental strategy and ORF as in the previous section to study the effect of EF-G concentration in a range of 0.25–10 μM on the translocation time, τ_{trans}, in standard polymix buffer [30]. The emergence of ribosomal complex D, by formation of fMH$_6$A$_6$[^{14}C]LY[^{3}H]Phe-tRNA^{Phe} in the A site at different incubation times after rapid mixing of a solution containing ribosomal complex A with a solution containing ternary complexes with Tyr-tRNA^{Tyr} and [^{3}H]Phe-tRNA^{Phe} and varying EF-G concentration, is shown in Fig. 2a. The variation of the translocation rate, k_{trans}, defined as the inverse of the translocation time, $1/\tau_{trans}$, with the EF-G concentration is shown in Fig. 2b (blue squares and fitted Michaelis–Menten curve). The curve fitting estimated k_{cat} and K_M for translocation as 22 ± 3 s^{-1} and 1.3 ±0.3 μM, respectively. These "long distance to AUG" experiments monitoring a translocation event 15 codons downstream from the initiation codon were complemented by "short distance to AUG" experiments under similar conditions. In the latter, translocation of the second (UAC, Tyr) and third (UUC, Phe) codons of the ORF from the P to the E and from the A to the P site, respectively, was monitored (Fig. 2c). Here, the A-complex solution (Fig. 1a) containing initiation complexes with [^{3}H]fMet-tRNA^{fMet} in the P site was rapidly mixed with a solution containing EF-G and ternary complexes with unlabeled Tyr-tRNA^{Tyr} and Phe-tRNA^{Phe}. During incubation, complex B was first formed with [^{3}H]fMet-Tyr-tRNA^{Tyr} in the A site. Complex C was then formed by translocation of the dipeptidyl-tRNA into the P site followed by the emergence of complex D with [^{3}H]fMet-Tyr-Phe-tRNA^{Phe} in the A site. By exclusion of Lys-tRNA^{Lys} from the reaction mixture, translation stopped after fMet-Tyr-Phe synthesis. The time-dependent extents of dipeptide and tripeptide formation were detected through separation by reversed-phase HPLC on a C18 column and online scintillation counting. This experiment allowed for estimation of the total tripeptide formation time, τ_{tot}, and the first peptide bond formation time, τ_{p1}. The second peptide bond formation time, τ_{p2}, was determined in a parallel reaction where a solution of ribosomes containing [^{3}H]fMet-Tyr-tRNA^{Tyr} in the P site (complex C) was mixed with a solution containing ternary complex with unlabeled Phe-tRNA^{Phe}. The translocation rates

obtained for the short ORF, $k_{trans} = 1/\tau_{trans}$, are plotted along with the data for the long ORF in Fig. 2b (black squares and fitted Michaelis–Menten curve). For the short ORF, the curve fitting estimated k_{cat} and K_M for translocation as 13 ± 4 s^{-1} and 2.5 ±1.3 μM, respectively.

Translocation rate variation with free Mg^{2+} concentration

In cell-free protein synthesis systems, the free magnesium ion (Mg^{2+}) concentration has a large impact on the accuracy of codon reading by tRNAs [18,30] and on the rate of mRNA movement in EF-G-driven translocation [20]. Here, we report on how the time of the full elongation cycle and its translocation part responded to varying free Mg^{2+} concentration in an interval of 1–6 mM at high (10 μM) and low (0.5 μM) concentration of EF-G. The experiments were mainly performed as described above (Fig. 1a) with a starting complex, A, containing fMH$_6$A$_6$[^{14}C]L-tRNA^{Leu} in the P site and a Tyr codon in the A site. At elevated Mg^{2+} concentration, it was not possible to form pre-elongated complexes *in situ*, presumably due to significant read-through of the aminoacyl-tRNA starved site. Complex A was therefore first formed in standard polymix buffer [30], where the read-through by missense errors was negligible. The standard buffer contained 5 mM total Mg^{2+} concentration that, together with the Mg^{2+}-chelating compounds ATP (1 mM), GTP (1 mM) and phosphoenol pyruvate (10 mM), resulted in approximately 1.3 mM free Mg^{2+} [18]. Complex A was purified by centrifugation through a sucrose cushion and used in ribosome mixtures, in which the Mg^{2+} concentration was increased by addition of extra Mg(OAc)$_2$ or decreased by addition of the chelating compound CTP (mM).

The elongation cycle rate decreased greatly as the free Mg^{2+} concentration increased from 1 to 6 mM due to a small decrease in the peptide bond formation rate and a large decrease in the translocation rate. The translocation rate at the different Mg^{2+} concentrations at high and low EF-G concentration is shown in Fig. 3. At near-saturating EF-G concentration (10 μM), the translocation rate decreased monotonically about 30-fold from its highest value of 32 s^{-1} at 1 mM to its lowest value of 1.2 s^{-1} at a concentration of 6 mM free Mg^{2+}. At low EF-G concentration (0.5 μM), the translocation rate first increased slightly from 8 to 12 s^{-1} as the Mg^{2+} concentration increased from 1 to 1.3 mM. Upon further increase of the Mg^{2+} concentration, the translocation rate decreased monotonically toward its smallest value of 1.2 s^{-1}, equal to the corresponding translocation rate at high EF-G concentration. This suggests that increasing Mg^{2+} concentration greatly decreased the *maximal* rate (k_{cat} value) of translocation and significantly decreased the concentration of EF-G at which the translocation rate was equal to half its maximal rate, that is, the K_m value.
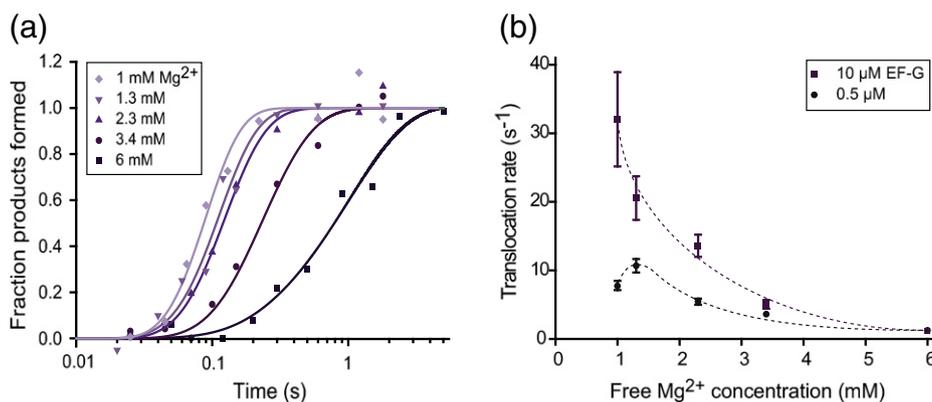
Fig. 3. Effect of the free Mg^{2+} concentration on the translocation rate in the long ORF. (a) Time courses for the three-step process of peptide bond formation, translocation and a second peptide bond formation at 10 μM EF-G and 1.5 μM ternary complex concentrations at varying free Mg^{2+} concentration (1–6 mM) The product formation yield did not vary significantly over this range of Mg^{2+} concentrations. (b) The translocation rate at near-saturating (10 μM, purple) and sub-saturating (0.5 μM, black) EF-G concentration plotted as a function of the free Mg^{2+} concentration in the buffer.

Is translocation slowed down by SD-like sequences in ORFs?

It was suggested from ribosomal profiling experiments with deep sequencing that the overall peptide elongation rate varied greatly with the free energy of interaction between SD-like sequences in ORFs of translated mRNAs and the anti-SD sequence of 16S rRNA [26]. To test if such interactions affect the rate of translocation at a site deep into an ORF, we designed three mRNA templates encoding the very same peptide with an N-terminal His-tag and a translocation site of study with a UAC (Tyr) codon and a UUC (Phe) codon at positions 15 and 16, respectively. In each ORF, codons 8–13 encoded the peptide sequence TTTEVTK, for which all codons were identical in all templates, except for codon 11 encoding Glu and codon 12 encoding Val. These two codons, situated in the SD-like sequence of the ORF, encoded Glu and Val as (GAG, GUU), (GAA, GUG) or (GAA, GUU) with SD–anti-SD interaction free energies estimated as −6.6, −2.3 or −0.4 kcal/mol (Fig. 4a). Using the method outlined above (Fig. 1a), the rate of translocation at high EF-G concentration (10 μM) was estimated for each of these three mRNA templates.

The starting complex, A in Fig. 1a, was a pre-elongated ribosome with the peptidyl-tRNA fMH$_6$T$_3$EVT[^{14}C]K-tRNA^{Lys} in the P site, where the ^{14}C-labeled lysine served as the internal standard. The quench-flow-synthesized peptides containing the subsequently encoded Tyr and Phe were isolated by nickel-affinity chromatography and the incorporation of radiolabeled amino acids was quantified by scintillation counting. Time curves for separate formation of the first (orange trace) and

the second (green trace) peptide bond and for the overall reaction including the first peptide bond formation, the translocation and the second peptide bond formation (blue trace) in the case of weak anti-SD–SD interaction (Fig. 4a; GAA and GUU in positions 11 and 12, respectively) are shown in Fig. 1b. The translocation rates for the three templates were indistinguishable and estimated as about 35 s^{-1}, and the peptide bond formation rates for the different templates were also uniform.

Discussion

Translocation has in the past mainly been studied with short mRNA templates at translocation sites close to the initiation site. However, translocation of initiator fMet-tRNA^{fMet} has been found to be slower than translocation of some elongator tRNAs [31,32]. To remove this possible artifact of experimental design, we developed a biochemical assay system to enable monitoring of the average time for the total cycle of mRNA and tRNA translocation on the bacterial ribosome at any position in any type of ORF (Fig. 1). Alternative methods to measure the translocation rate include fluorescence labeling of mRNA [11], fluorescence labeling of tRNA [13], fluorescence labeling of ribosomal subunits [12] and probing of the post-translocation complex with puromycin [33,34]. As demonstrated, for example, by Holtkamp *et al.* [28], Cunha *et al.* [33] and Savelsbergh *et al.* [35], these approaches estimate but fractions of the total translocation time and the mechanistic interpretation of the results is sometimes difficult. For instance, Cunha *et al.* used one and the same mRNA labeled with two different
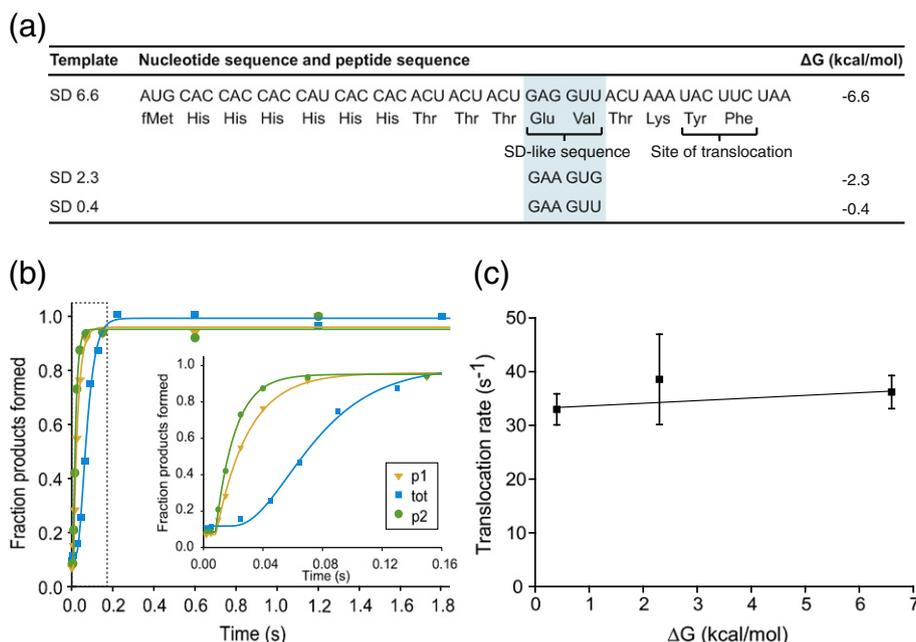
(a)

Template	Nucleotide sequence and peptide sequence	ΔG (kcal/mol)
SD 6.6	AUG CAC CAC CAC CAU CAC CAC ACU ACU ACU GAG GUU ACU AAA UAC UUC UAA fMet His His His His His His Thr Thr Thr Glu Val Thr Lys Tyr Phe	-6.6
	SD-like sequence Site of translocation	
SD 2.3	GAA GUG	-2.3
SD 0.4	GAA GUU	-0.4

(b) (c)

Fig. 4. Dependency of the translocation rate on the strength of interaction between an upstream SD-like sequence and the anti-SD sequence. (a) The nucleotide sequences of the ORF of the mRNAs containing SD-like sequences upstream of the translocation site. All templates code for the same peptide sequence but have different codons at the SD-like sequence site. The affinity of the SD-like sequence for the anti-SD sequence (as determined by free energy calculations) is indicated on the right. (b) Time courses for the three reactions in a translocation experiment, the overall three-step reaction (blue trace), first peptide bond formation (orange trace) and second peptide bond formation (green trace) obtained using the SD0.4 mRNA template at 10 μM EF-G and 1.5 μM ternary complex concentrations. Fitting of the data to the three-step model gave τ_{p1} = 30 ± 2 ms, τ_{p2} = 21 ± 1 ms and τ_{trans} = 28 ± 3 ms. The inset shows the first 160 ms of the reactions in magnification as indicated by the broken line. (c) Translocation rates obtained at 10 μM EF-G for the three templates in (a) plotted as a function of the affinity for the anti-SD sequence. Each point is the average of results from two or three individual measurements.

fluorophores but they unexpectedly estimated one very short time (30 ms) and one remarkably long time (167 ms) instead of monitoring the same time for mRNA movement.

Here, our novel assay system was used to estimate the total translocation time from EF-G association to the pre-translocation ribosome to EF-G dissociation from the post-translocation ribosome in strategically chosen contexts of biological relevance. Not surprisingly, we found translocation to be significantly slower when a two-codon translocation site was at positions 2 and 3 than at positions 15 and 16 in an ORF (Fig. 2).

The minimal translocation time at near-saturating EF-G concentration ($\approx 1/k_{cat}$) for a translocation site, 15 codons downstream of the initiation codon (AUG), displayed great variation with the concentration of free Mg^{2+} ions in our polymix buffer system. At a physiologically relevant concentration of free Mg^{2+} (see also below) [36], the translocation rate at 10 μM EF-G was approximately 30 s^{-1} and decreased sharply with increasing Mg^{2+} concentration to about 1 s^{-1} at 6 mM free Mg^{2+} (Fig. 3). The translocation rate at a 20-fold lower EF-G concen-

tration (0.5 μM) increased slightly from about 7 to 10 s^{-1} with the initial increase of Mg^{2+} concentration and then dropped to a rate of about 1 s^{-1}, identical with that at 10 μM EF-G, as the Mg^{2+} concentration increased further to 6 mM. This means that the translocation rate at 10 μM EF-G was near maximal at all Mg^{2+} concentrations used here and, furthermore, that the K_m value for EF-G interaction with the pre-translocation ribosome decreased from about 1.9 μM at 1 mM Mg^{2+} to a value smaller than 0.5 μM at 6 mM Mg^{2+}. The simplest way to account for these data is that the K_m decrease with increasing Mg^{2+} concentration was due to a large decrease of the maximal translocation rate, k_{cat}, at an unaltered k_{cat}/K_M, for example by an unchanged rate constant, k_a, for EF-G association to the pre-translocation ribosome and a dissociation rate constant from the initial complex between EF-G and the ribosome, k_d, always much smaller than the forward rate constant, k_f, from this complex:

$$K_m = \frac{k_f + k_d}{k_a k_f} k_{cat} \approx \frac{k_{cat}}{k_a}$$

In this scenario, EF-G binding to the pre-translocation ribosome led to completed translocation with a probability close to one at all Mg^{2+} concentrations. The constant k_a value was about 20 μM^{-1} s^{-1}, an estimate about 10-fold smaller than earlier bulk estimates [37] and about 10-fold larger than earlier single-molecule estimates [14].

What, then, could have caused the reduction in k_{cat} by increasing Mg^{2+} concentration as observed in the present work (Fig. 4)? It was pointed out by Gao *et al.* [38] that the tip of domain IV of EF-G, loop I, may be in contact with both the A -site codon and the peptidyl-tRNA already in the pre-translocation ribosome. This contact may, furthermore, remain intact during translocation of the A -site codon and the peptidyl-tRNA into the P site. Therefore, an early event in translocation is likely to be the displacement by loop I of the "monitoring bases" G530, A1492 and A1493 that line the minor groove of the codon–anticodon helix during decoding [39]. This would neatly explain why small inhibitors of protein synthesis that stabilize the minor groove interactions of the "monitoring bases" greatly reduce the rate of translocation [40]. We have previously observed strong Mg^{2+} concentration dependence of the accuracy of codon reading [18], suggesting that the evolutionary stability of genetic code translation requires a much smaller concentration of free Mg^{2+} than normally used in biochemical assay systems. It was recently proposed [41] with support from structural [42] and kinetics [43,44] data that also Mg^{2+} ions stabilize the minor groove interactions of the monitoring bases. This attractive proposition would offer a unified explanation for the error-inducing effects of antibiotics and Mg^{2+} ions and for their inhibitory action on translocation as seen here and earlier [20]. In line with this, we suggest that the strong, Mg^{2+} concentration-dependent inhibition of translocation shown in Fig. 3 was due to increasing stabilization of the monitoring bases in the minor groove of the codon–anticodon helix by increasing occupation of strategic sites for Mg^{2+} binding [42].

Together, these findings suggest that both high accuracy of codon recognition by tRNAs and rapid peptide elongation in the context of the polymix buffer system [30,45] required a much lower Mg^{2+} concentration than normally used in past and present biochemical assays. This makes the relevance of previous *in vitro* data problematic and *in vivo* modeling of protein synthesis based on such data difficult. The present study shows, however, that this lack of *in vivo* compatibility is not an intrinsic property of *in vitro* systems but can easily be removed by properly tuned reaction conditions and factor concentrations.

From recent ribosomal profiling experiments on *E. coli* cells by Li *et al.* [26], it was suggested that the local peptide elongation rate does not vary with the concentrations of tRNA isoacceptors but only with the strength of interaction between SD-like sequences in ORFs and the anti-SD sequence of the 16S rRNA in the 30S subunit of the translating ribosome. The lack of positive correlation between tRNA isoacceptor concentration and peptide elongation rate [26] has remarkable implications. According to the law of mass action, the rate of association of a particular tRNA isoacceptor to ribosomes programmed with its cognate codons is proportional to the concentration of its corresponding ternary complex with EF-Tu and GTP [21]. Given this fact, the profiling result suggests that the times of association of tRNA isoacceptors in ternary complex are negligible compared to the times to complete the other parts of the elongation cycle, including peptidyl transfer and translocation. Alternatively, differences in ternary complex binding time are neutralized by other factors that affect the tRNA association times [21]. One obvious possibility is that internal SD sequences slow down the speed of translocation of mRNA. In the present work, we aimed at a direct test under *in vivo*-like conditions of the hypothesis that internal SD-like sequences of varying free energy of interaction with the anti-SD sequence of 16S rRNA will reduce the speed of translocation. We found no difference in the rate of translocation among three SD-like sequences of different strengths separated from the translocation site by two codons (6 nt) (Fig. 4c). In this case, there was virtually no inhibition of the translocation rate by the varying SD–anti-SD interaction strength. Interestingly, recently obtained single-molecule data [27] suggest a 2-fold increase in the lifetime (from 5 to 12 s) of the ratcheted ribosomal state by the presence of an internal SD sequence (– 6.1 kcal/mol) separated from the translocation site by 7 nt, similar to the 6-nt separation of the present work (Fig. 4a). We note that the time scale in the single-molecule experiments (≈ 5 s) is 2 orders of magnitude longer than the time scale in the present work (≈ 30 ms) and the time scale of elongation *in vivo* [5].

An extended testing of the hypothesis that internal SD sequences slow down the peptide elongation cycle [26] and the corollary that such a slowing down is due to inhibition of translocation remains to be performed. It will require experiments in which the distance between the translocation site and the SD-like sequence is systematically varied in different mRNA sequence contexts. For this, the *in vivo*-like properties of the assay system developed here will be essential.

Regarding systems biology modeling of growing bacteria with implications for optimal physiology of growth [46,47], growth inhibition by antibiotics [48], fitness loss by drug resistance mutations and improved fitness by compensatory mutations [49], quantitative assessment of the kinetic properties of the protein synthesis machinery is essential. One reason is that ribosomes and their factor proteins

occupy a significant fraction of the bacterial proteome [46,47], making cell growth and fitness hypersensitive to ribosome performance so that calibration of the biochemistry of protein synthesis to ribosome performance *in vivo* is a prerequisite for realistic systems biology modeling of bacterial cell growth. Such a calibration is a multiple parameter problem, but the present and earlier [18,29,50] work suggest that the concentration of free Mg^{2+} ions plays such an important role that adjustment of this parameter is the natural starting point for such a calibration. As indicated above, high Mg^{2+} concentration favors the interactions of the monitoring bases [41] with the minor grove of the codon–anticodon helix [39,51], thereby facilitating ternary complex binding to the ribosome and subsequent GTP hydrolysis for cognate and non-cognate ternary complex alike [18,43,52]. This accounts for the increase in amino acid substitution error [18] and the enhanced inhibition of protein synthesis by non-cognate ternary complex [29,43,50,52] in response to increased Mg^{2+} concentration. By the same mechanism, low Mg^{2+} concentration leads to low frequency of amino acid substitution errors in conjunction with inefficient binding to the ribosome and slow GTP hydrolysis for cognate and non-cognate ternary complex. This accounts for the efficiency–accuracy trade-off for genetic code translation [18,46,50]. In conclusion, a free Mg^{2+} concentration of about 1 mM in our polymix buffer system makes our biochemistry near *in vivo* compatible with respect to ribosome speed (Fig. 3) and accuracy [18] of genetic code translation. We are therefore optimistic that protein synthesis carried out in cell-free systems under optimal conditions may serve as a suitable basis for systems biology modeling of bacterial physiology with implications for bacterial physiology, antibiotic resistance development and molecular evolution.

Materials and Methods

Reagents and reaction conditions

Ribosomes (*E. coli* MRE600) were prepared according to Johansson *et al.* [29]. fMet-tRNA^{fMet} was prepared as described by Antoun *et al.* [53], with minor modifications. Initiation factors (IF) and elongation factors were over-expressed His-tagged and purified by nickel-affinity chromatography on a 5-ml HiTrap column from GE Healthcare. tRNA^{Tyr} and tRNA^{Phe} were from Chemical Block (Russia). Bulk tRNA was prepared according to the principle of Kelmers *et al.* [54]. Radiolabeled amino acids were from Biotrend (Germany). Nickel-NTA agarose was from Qiagen. GTP, CTP and ATP were from Amersham Biosciences. All other chemicals were from Merck or Sigma Aldrich.

mRNA templates were prepared by transcription from double-stranded DNA synthesized by extension of single-stranded DNA primers with overlapping sequences by PCR

essentially as described by Antoun *et al.* [53]. Preparation of the transcription reaction mixture and purification of the mRNA on poly-dT column was performed as described by Pavlov *et al.* [55] with minor modifications. The same forward primer was used to prepare all mRNAs and had the sequence (from 5′ to 3′) GGTACCGAAATTAATACGACT CACTATAGGGAATTCGGGCCCTTGTTAACAATTAAG GAGG. It was annealed to either of the reverse primers, firstly for making fMYF mRNA (short ORF) TTTTTTTTTTTTTTTT TTTTTCTGCAATTAATGATGATGATGATGGTGTGCTGC TGCTGCTGCTGCTTTGAAGTACATTTAATACCTCCT TAATTGTTAACAAGGGCCCG or secondly for making fMH$_6$A$_6$LYF mRNA (long ORF) TTTTTTTTTTTTTTTT TTTTTCTGCAATTAGAAGTACAGTGCTGCTGCTGCTG CTGCATGATGATGATGATGGTGCATTTAATACCTCCT TAATTGTTAACAAGGGCCCG (overlaps are underlined), and for the SD6.6 mRNA: TTTTTTTTTTTTTTTT TTTTTCTGCAATTAGAAGTATTTAGT**AACCTC**AGTAG TAGTGTGGTGATGGTGGTGGTGCATTTAATACCTCCT TAATTGTTAACAAGGGCCCG (residues marked in bold are varied for the other mRNAs of the SD series according to the following: SD2.3: **CACTTC** and SD0.4: **AACTTC**). The interaction free energies between the SD-like sequence and the anti-SD sequence were calculated using the Vienna RNA software[†].

All experiments were performed in polymix buffer [95 mM KCl, 5 mM NH$_4$Cl, 0.5 mM CaCl$_2$, 8 mM putrescine, 1 mM spermidine, 5 mM potassium phosphate, 1 mM dithioerythritol and 5 mM Mg(OAc)$_2$] at 37 °C. Extra Mg(OAc)$_2$ or CTP was added to adjust the free magnesium concentration of the buffer where indicated. An energy regeneration system consisting of 1 mM ATP, 1 mM GTP, 10 mM phosphoenol pyruvate, 50 μg/ml pyruvate kinase and 2 μg/ml myokinase was present in all reaction mixtures. All concentrations given for translation factors in the reaction mixtures were determined by the Bradford assay.

Translocation assay for the long ORF template

To measure the rate of a translocation step inside a long ORF, we needed three parallel quench-flow reactions: one where the total time of the first peptide bond formation, the translocation and the second peptide bond formation was measured (TOT); one for the first peptide bond formation (P1); and one for the second peptide bond formation (P2). For each reaction, an initiation mixture, a pre-elongation mixture and a translation factor mixture were needed. The initiation mixture was common to all three reactions and contained ribosomes (1 μM, whereof 70% were active in dipeptide formation), fMH$_6$A$_6$LYF mRNA (8 μM), unlabeled initiator fMet-tRNA^{fMet} (1.5 μM), IF1 (2 μM), IF2 (1 μM) and IF3 (2 μM). Three pre-elongation mixtures (P1, TOT and P2) were prepared, all containing EF-Tu (8 μM), EF-Ts (0.8 μM), EF-G (0.2 μM), tBulk (260 μM total tRNA, whereof tRNA^{His} constituted 1.8 μM), ^{14}C leucine (20 μM), alanine (400 μM), histidine (400 μM), LeuRS (0.2 μM), AlaRS (1 μM) and HisRS (2.5 μM). In addition, the P2 pre-elongation mixture contained TyrRS (1.5 μM) and tyrosine (20 μM). Three translocation mixtures were also prepared containing tRNA^{Tyr} (3 μM), tRNA^{Phe} (3 μM), EF-Tu (22 μM), EF-Ts (2 μM), EF-G (0.5–20 μM as indicated) and PheRS (1.2 μM). In addition to this, the P1 translation factor mixture contained ^{3}H-tyrosine

(20 μM), unlabeled phenyl alanine (20 μM) and TyrRS (1.5 μM); the TOT translation factor mixture contained unlabeled tyrosine (20 μM), ^{3}H-phenyl alanine (20 μM) and TyrRS (1.5 μM); and the P2 translation factor mixture contained unlabeled tyrosine (20 μM), ^{3}H-phenyl alanine (20 μM) and TyrRS (0.75 μM). All reaction mixtures were incubated for 15 min at 37 °C. Each pre-elongation mixture was then mixed with an equal volume of initiation mixture and the resulting ribosome complex mixtures were incubated for another 2 min to allow for the formation of the fMH$_6$A$_6$[^{14}C]L peptide (P1 and TOT) or the fMH$_6$A$_6$[^{14}C]LY peptide (P2). All mixtures were kept on ice until loaded into the quench-flow instrument. Equal volumes of each ribosome complex mixture (P1, TOT and P2) were rapidly mixed with equal volumes of the corresponding translation factor mixture in a quench-flow instrument (RQF-3; KinTek, Corp.) at 37 °C and quenched with 50% formic acid after different times of incubation. Precipitates formed upon quenching were collected by centrifugation at 20,800g for 15 min. The peptides were isolated by nickel-affinity chromatography as described below.

Isolation of peptides by nickel-affinity chromatography

The precipitate from each quench-flow sample was resuspended in 100 μl of 0.5 M KOH by vortexing and incubation at room temperature for 10 min. We added 500 μl NPI0 buffer (50 mM NaH$_2$PO$_4$ and 300 mM NaCl) to each sample. We then loaded 580 μl from each sample onto 100 μl nickel-NTA agarose pre-equilibrated with NPI0 buffer in columns in a VacMaster device (IST). Binding was allowed for 2 min before the liquid was removed by application of vacuum. The resin was washed five to seven times by application of 1 ml NPI20 buffer (50 mM NaH$_2$PO$_4$, 300 mM NaCl and 20 mM imidazol) to each column. The peptides were eluted by application of 600 μl NPI500 buffer (50 mM NaH$_2$PO$_4$, 300 mM NaCl and 500 mM imidazol). From the eluate fractions, 550 μl was transferred to scintillation vials and 5 ml of scintillation cocktail was applied (Quicksafe flow 2; Zinsser Analytic). The amount of incorporated ^{3}H-labeled amino acids and the amount of the ^{14}C-labeled internal standard in each eluate fraction were determined by scintillation counting (LS6500; Beckman Coulter) in two different energy windows (0–200 and 400–700 keV).

Translocation assay for the short ORF template

To measure the rate of the translocation step between the second and the third codon, we needed two reactions, one where the formation of dipeptide and tripeptide (f[^{3}H]MY and f[^{3}H]MYF) on ribosomes initiated with [^{3}H]fMet-tRNA^{fMet} was followed (P1/TOT) and one where the formation of tripeptide on ribosomes having a [^{3}H]fMY dipeptidyl-tRNA in the P site was followed (P2). The initiation mixture was common to the two reactions and identical with the case of translocation in a long ORF described above except for the use of fMYF mRNA (8 μM) and labeled ^{3}H-fMet-tRNA^{fMet} (1.2 μM). Two pre-elongation mixtures were prepared without (P1/TOT) and with tyrosyl-tRNA synthetase (TyrRS) (1.5 μM) and tyrosine (20 μM) (P2). Apart from this, they were identical with the pre-elongation mixtures in the long ORF case except that

^{14}C-labeled leucine was replaced by unlabeled leucine. Two translation factor mixtures were prepared containing TyrRS (1.5 μM) and unlabeled tyrosine (20 μM) (P1/TOT) and TyrRS (0.75 μM) and tyrosine (10 μM) (P2). Apart from this, both of them contained unlabeled Phe (20 μM) and tRNAs, elongation factors and PheRS at the same concentrations as for the long ORF case. All reaction mixtures were incubated for 15 min at 37 °C. Each pre-elongation mixture was then mixed with an equal volume of initiation mixture and the resulting ribosome complex mixtures were incubated for another 2 min. All reaction mixtures were then kept on ice. Equal volumes of the each ribosome complex mixture and the corresponding translocation mixture were rapidly mixed in a quench-flow instrument at 37 °C and quenched with 50% formic acid after different incubation times. The precipitates were collected by centrifugation at 20,800g for 15 min. The supernatants were removed and each pellet was resuspended in 165 μl of 0.5 M KOH by vortexing and incubation at room temperature for 10 min to ensure hydrolysis of the bond between the peptide and the tRNA. We added 13 μl of 100% formic acid and centrifuged the samples two times at 20,800g for 15 min, with transfer into new tubes between centrifugations, to ensure the removal of all precipitate. The amounts of f[^{3}H]Met, dipeptide f[^{3}H]MY and tripeptide f[^{3}H]MYF were determined by reversed-phase HPLC on a C18 column (Merck) with isocratic elution in a buffer consisting of 30% methanol and 0.1% TFA in water and with online scintillation counting (β-RAM Model 3; IN/US Systems).

Preparation of purified pre-elongated complexes for Mg^{2+} titration experiments

To prepare the pre-elongated complexes for the Mg^{2+} titration experiments, we prepared an initiation mixture containing ribosomes (5 μM), YF1516 mRNA (50 μM), initiator ^{3}H-fMet-tRNA^{fMet} (8.3 μM), IF1 (5 μM), IF2 (3.3 μM) and IF3 (5 μM). Two pre-elongation mixtures were prepared without and with tyrosyl-tRNA synthetase (TyrRS) (1.1 μM) and tyrosine (29 μM) (700 μl and 350 μl, respectively). Both mixtures contained EF-Tu (21 μM), EF-Ts (2.9 μM), EF-G (1.4 μM), tBulk (630 μM total tRNA from OD$_{260}$ measurement), ^{14}C-labeled leucine (14 μM), alanine (290 μM), histidine (290 μM), LeuRS (0.13 μM), AlaRS (0.7 μM) and HisRS (1.8 μM). All mixtures were incubated at 37 °C for 15 min. Initiation mixture (300 μl and 150 μl, respectively) was added to the pre-elongation mixtures and the reaction mixtures were incubated for another 2 min to let the peptides form. The reaction mixtures (500 μl) were loaded onto sucrose cushion (1.1 M sucrose in polymix buffer, 400 μl) and ultra-centrifuged (Sorvall, RC M150 GX) in an S55S swing-out rotor at 259,000g at 4 °C for 2 h. The resulting pellets containing the pre-elongated ribosome complexes were washed with 200 μl of polymix and resolved in 50 μl polymix each. The pre-elongated complexes were shock frozen in liquid nitrogen and stored at −80 °C.

Effect of Mg^{2+} concentration on the translocation rate

For Mg^{2+} titration experiments, the initiation and pre-elongation mixtures were replaced by a ribosome

complex mixture containing the pre-elongated complexes at 0.5 µM concentration. The factor concentrations in the elongation mixtures were identical with those described above for translocation rate determination in the long ORF. To all ribosome complex mixtures and elongation mixtures, we added $Mg(OAc)_2$ (up to 8 mM extra) or CTP (0.5 mM) to adjust the free Mg^{2+} ion concentration resulting in a free magnesium concentration of 1–6 mM. Only the elongation mixtures (not the ribosome complex mixture) were incubated 15 min at 37 °C. Reactions were carried out in a quench-flow instrument and the samples were treated as described above for translocation experiments in a long ORF.

Effect of SD-like sequences on the translocation rate

The translocation rates on the SD templates were determined using the general method for determining the translocation rate in a long ORF described above, with modifications of the composition of the pre-elongation mixture due to the different sequence of the encoded peptide. The initiation mixture was identical with what was described above, except that the mRNA was replaced by either of the SD mRNAs. The three pre-elongation mixtures (P1, TOT and P2) all contained EF-Tu (10 µM), EF-Ts (1 µM), EF-G (0.2 µM), tBulk (260 µM), ^{14}C-lysine (20 µM), threonine (400 µM), histidine (400 µM), glutamic acid (400 µM), valine (400 µM), LysRS (1.8 µM), ThrRS (2 µM), HisRS (2.5 µM), GluRS (2.6 µM) and ValRS (1 µM). In addition, the P2 pre-elongation mixture contained TyrRS (1.5 µM) and tyrosine (20 µM). The elongation mixtures were identical with the long ORF case mentioned above. All incubation steps and the peptide isolation and so on were performed as described previously.

Data analysis

For each translocation experiment, three time courses were obtained. For each time point, the ^{14}C and ^3H emission was determined by scintillation counting in two energy windows. The 400–700 keV window contained only the ^{14}C signal and the 0–200 keV window contained mainly the ^3H signal. However, due to overlap of the ^3H and ^{14}C signals, 10% of the ^{14}C signal in the 400–700 window had to be subtracted as background from the 0–200 window. The ^3H signal of each sample was then weighted by the ^{14}C signal to compensate for any variation in peptide recovery during sample treatment, according to the following:

Weighted ^3H signal

$$= \frac{^3H \text{ signal of sample X} \cdot {}^{14}C \text{ signal average of all samples}}{^{14}C \text{ signal of sample X}}$$

(1)

The data were fitted to a model where ribosome complex A was converted by three irreversible steps, corresponding to two peptide bond formation steps and translocation separated by a translocation step, into ribosomal complex D:

$$A \xrightarrow{k_{p1}} B \xrightarrow{k_{trans}} C \xrightarrow{k_{p2}} D$$
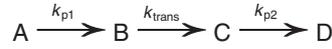
Here, each rate constant (k) is the inverse of the average time to perform that step, according to:

$$\tau_{p1} = \frac{1}{k_{p1}}, \tau_{trans} = \frac{1}{k_{trans}} \text{ and } \tau_{p2} = \frac{1}{k_{p2}} \quad (2)$$

The peptide bond formation reactions displayed single exponential behavior with an initial delay equal to t_{delay}. They were fitted to the following equation [given for the A-to-B conversion (τ_{p1}), but the same type of expression is valid for the C-to-D conversion (τ_{p2})]:

$$b = a_1 \cdot \left(1 - e^{-(t-t_{delay1})/\tau_{p1}}\right) + bg_1 \quad (3)$$

For the delay region, the function was equal to the background level [bg_1 in Eq. (3)]. The equation for formation of complex D from complex A is more complex:

$$d = \frac{a_2}{\tau_{p1}\tau_{trans}\tau_{p2}\left(\frac{1}{\tau_{trans}} - \frac{1}{\tau_{p1}}\right)}$$

$$\times \left(\frac{\tau_{p2}\left(e^{-(t-t_{delay1}-t_{delay2})/\tau_{p2}} - 1\right) - \tau_{p1}\left(e^{-(t-t_{delay1}-t_{delay2})/\tau_{p1}} - 1\right)}{\frac{1}{\tau_{p2}} - \frac{1}{\tau_{p1}}} \right.$$

$$\left. - \frac{\tau_{p2}\left(e^{-(t-t_{delay1}-t_{delay2})/\tau_{p2}} - 1\right) - \tau_{trans}\left(e^{-(t-t_{delay1}-t_{delay2})/\tau_{trans}} - 1\right)}{\frac{1}{\tau_{p2}} - \frac{1}{\tau_{trans}}} \right)$$

$$+ bg_2$$

(4)

Here, the length of delay time was fitted as the sum of the delays of the two peptide formation reactions and set equal to the background [bg_2 in Eq. (4)]. The three time courses from one translocation experiment were fitted jointly sharing the time constants (τ_{p1}, τ_{trans} and τ_{p2}). The curve fit errors were obtained as sigma values for each of the parameters. All translocation experiments were repeated twice or more and the parameter estimates were averaged by weighting each value by its corresponding variance according to:

$$k = \frac{\sum_{i=1}^{n} w_i \cdot k_i}{\sum_{i=1}^{n} w_i} \quad (5)$$

and the average standard deviation was calculated as

$$\sigma_k = \frac{1}{\sqrt{\sum_{i=1}^{n} w_i}} \text{ where } w_i = \frac{1}{\sigma_{k_i}^2} \quad (6)$$

Acknowledgements

References

[1] Young R, Bremer H. Polypeptide-chain-elongation rate in *Escherichia coli* B/r as a function of growth rate. Biochem J 1976;160:185–94.

[2] Proshkin S, Rahmouni AR, Mironov A, Nudler E. Cooperation between translating ribosomes and RNA polymerase in transcription elongation. Science 2010;328:504–8.

[3] Liang ST, Xu YC, Dennis P, Bremer H. mRNA composition and control of bacterial gene expression. J Bacteriol 2000; 182:3037–44.

[4] Schmeing TM, Ramakrishnan V. What recent ribosome structures have revealed about the mechanism of translation. Nature 2009;461:1234–42.

[5] Bremer H, Dennis P. Modulation of chemical composition and other parameters of the cell by growth rate. In: Neidhardt FC, editor. *Escherichia coli* and *Salmonella*: Cellular and Molecular Biology 2. Washington, DC: ASM Press; 1996. p. 1553–69.

[6] Brunschede H, Bremer H. Synthesis and breakdown of proteins in *Escherichia coli* during amino-acid starvation. J Mol Biol 1971;57:35–57.

[7] Goldberg AL, Dice JF. Intracellular protein degradation in mammalian and bacterial cells. Annu Rev Biochem 1974;43: 835–69.

[8] Goldberg AL, St John AC. Intracellular protein degradation in mammalian and bacterial cells: part 2. Annu Rev Biochem 1976;45:747–803.

[9] Rodnina MV, Savelsbergh A, Katunin VI, Wintermeyer W. Hydrolysis of GTP by elongation factor G drives tRNA movement on the ribosome. Nature 1997;385:37–41.

[10] Valle M, Zavialov A, Sengupta J, Rawat U, Ehrenberg M, Frank J. Locking and unlocking of ribosomal motions. Cell 2003;114:123–34.

[11] Studer SM, Feinberg JS, Joseph S. Rapid kinetic analysis of EF-G-dependent mRNA translocation in the ribosome. J Mol Biol 2003;327:369–81.

[12] Ermolenko DN, Majumdar ZK, Hickerson RP, Spiegel PC, Clegg RM, Noller HF. Observation of intersubunit movement of the ribosome in solution using FRET. J Mol Biol 2007;370: 530–40.

[13] Pan D, Kirillov SV, Cooperman BS. Kinetically competent intermediates in the translocation step of protein synthesis. Mol Cell 2007;25:519–29.

[14] Chen J, Petrov A, Tsai A, O'Leary SE, Puglisi JD. Coordinated conformational and compositional dynamics drive ribosome translocation. Nat Struct Mol Biol 2013;20: 718–27.

[15] Brune M, Hunter JL, Corrie JE, Webb MR. Direct, real-time measurement of rapid inorganic phosphate release using a novel fluorescent probe and its application to actomyosin subfragment 1 ATPase. Biochemistry 1994;33:8262–71.

[16] Rodnina MV, Savelsbergh A, Matassova NB, Katunin VI, Semenkov YP, Wintermeyer W. Thiostrepton inhibits the turnover but not the GTPase of elongation factor G on the ribosome. Proc Natl Acad Sci USA 1999;96:9586–90.

[17] Cornish PV, Ermolenko DN, Noller HF, Ha T. Spontaneous intersubunit rotation in single ribosomes. Mol Cell 2008;30: 578–88.

[18] Johansson M, Zhang J, Ehrenberg M. Genetic code translation displays a linear trade-off between efficiency and accuracy of tRNA selection. Proc Natl Acad Sci USA 2012;109:131–6.

[19] Kurland CG, Ehrenberg M. Optimization of translation accuracy. Prog Nucleic Acid Res Mol Biol 1984;31:191–219.

[20] Feldman MB, Terry DS, Altman RB, Blanchard SC. Aminoglycoside activity observed on single pre-translocation ribosome complexes. Nat Chem Biol 2010;6:244.

[21] Berg OG, Kurland CG. Growth rate-optimised tRNA abundance and codon usage. J Mol Biol 1997;270:544–50.

[22] Zhang G, Hubalewska M, Ignatova Z. Transient ribosomal attenuation coordinates protein synthesis and co-translational folding. Nat Struct Mol Biol 2009;16:274–80.

[23] Stadler M, Fire A. Wobble base-pairing slows *in vivo* translation elongation in metazoans. RNA 2011;17:2063–73.

[24] Ingolia NT, Lareau LF, Weissman JS. Ribosome profiling of mouse embryonic stem cells reveals the complexity and dynamics of mammalian proteomes. Cell 2011;147: 789–802.

[25] Zinshteyn B, Gilbert WV. Loss of a conserved tRNA anticodon modification perturbs cellular signaling. PLoS Genet 2013;9:e1003675.

[26] Li GW, Oh E, Weissman JS. The anti-Shine-Dalgarno sequence drives translational pausing and codon choice in bacteria. Nature 2012;484:538–41.

[27] Chen J, Petrov A, Johansson M, Tsai A, O'Leary SE, Puglisi JD. Dynamic pathways of −1 translational frameshifting. Nature 2014;512:328–32.

[28] Holtkamp W, Cunha CE, Peske F, Konevega AL, Wintermeyer W, Rodnina MV. GTP hydrolysis by EF-G synchronizes tRNA movement on small and large ribosomal subunits. EMBO J 2014;33:1073–85.

[29] Johansson M, Bouakaz E, Lovmar M, Ehrenberg M. The kinetics of ribosomal peptidyl transfer revisited. Mol Cell 2008;30:589–98.

[30] Jelenc PC, Kurland CG. Nucleoside triphosphate regeneration decreases the frequency of translation errors. Proc Natl Acad Sci USA 1979;76:3174–8.

[31] Ermolenko DN, Noller HF. mRNA translocation occurs during the second step of ribosomal intersubunit rotation. Nat Struct Mol Biol 2011;18:457–62.

[32] Dorner S, Brunelle JL, Sharma D, Green R. The hybrid state of tRNA binding is an authentic translation elongation intermediate. Nat Struct Mol Biol 2006;13:234–41.

[33] Cunha CE, Belardinelli R, Peske F, Holtkamp W, Wintermeyer W, Rodnina MV. Dual use of GTP hydrolysis by elongation factor G on the ribosome. Translation 2013;1. http://dx.doi.org/10.4161/trla.24315.

[34] Semenkov Y, Shapkina T, Makhno V, Kirillov S. Puromycin reaction for the A site-bound peptidyl-tRNA. FEBS Lett 1992; 296:207–10.

[35] Savelsbergh A, Katunin VI, Mohr D, Peske F, Rodnina MV, Wintermeyer W. An elongation factor G-induced ribosome rearrangement precedes tRNA-mRNA translocation. Mol Cell 2003;11:1517–23.

[36] Alatossava T, Jutte H, Kuhn A, Kellenberger E. Manipulation of intracellular magnesium content in polymyxin B nonapeptide-sensitized *Escherichia coli* by ionophore A23187. J Bacteriol 1985;162:413–9.

[37] Katunin VI, Savelsbergh A, Rodnina MV, Wintermeyer W. Coupling of GTP hydrolysis by elongation factor G to translocation and factor recycling on the ribosome. Biochemistry 2002;41:12806–12.

[38] Gao YG, Selmer M, Dunham CM, Weixlbaumer A, Kelley AC, Ramakrishnan V. The structure of the ribosome with elongation factor G trapped in the posttranslocational state. Science 2009;326:694–9.

[39] Ogle JM, Brodersen DE, Clemons WM, Tarry MJ, Carter AP, Ramakrishnan V. Recognition of cognate transfer RNA by the 30S ribosomal subunit. Science 2001;292:897–902.

[40] Peske F, Savelsbergh A, Katunin VI, Rodnina MV, Wintermeyer W. Conformational changes of the small ribosomal subunit during elongation factor G-dependent tRNA-mRNA translocation. J Mol Biol 2004;343:1183–94.

[41] Satpati P, Sund J, Aqvist J. Structure-based energetics of mRNA decoding on the ribosome. Biochemistry 2014;53:1714–22.

[42] Demeshkina N, Jenner L, Westhof E, Yusupov M, Yusupova G. A new understanding of the decoding principle on the ribosome. Nature 2012;484:256–9.

[43] Gromadski KB, Daviter T, Rodnina MV. A uniform response to mismatches in codon-anticodon complexes ensures ribosomal fidelity. Mol Cell 2006;21:369–77.

[44] Pape T, Wintermeyer W, Rodnina MV. Conformational switch in the decoding region of 16S rRNA during aminoacyl-tRNA selection on the ribosome. Nat Struct Biol 2000;7: 104–7.

[45] Wagner EG, Jelenc PC, Ehrenberg M, Kurland CG. Rate of elongation of polyphenylalanine *in vitro*. Eur J Biochem 1982; 122:193–7.

[46] Ehrenberg M, Kurland CG. Costs of accuracy determined by a maximal growth rate constraint. Q Rev Biophys 1984;17: 45–82.

[47] Pavlov MY, Ehrenberg M. Optimal control of gene expression for fast proteome adaptation to environmental change. Proc Natl Acad Sci USA 2013;110:20527–32.

[48] Zorzet A, Pavlov MY, Nilsson AI, Ehrenberg M, Andersson DI. Error-prone initiation factor 2 mutations reduce the fitness cost of antibiotic resistance. Mol Microbiol 2010;75: 1299–313.

[49] Pavlov MY, Zorzet A, Andersson DI, Ehrenberg M. Activation of initiation factor 2 by ligands and mutations for rapid docking of ribosomal subunits. EMBO J 2011;30:289–301.

[50] Lovmar M, Ehrenberg M. Rate, accuracy and cost of ribosomes in bacterial cells. Biochimie 2006;88:951–61.

[51] Yoshizawa S, Fourmy D, Puglisi JD. Recognition of the codon-anticodon helix by ribosomal RNA. Science 1999;285: 1722–5.

[52] Gromadski KB, Rodnina MV. Kinetic determinants of high-fidelity tRNA discrimination on the ribosome. Mol Cell 2004; 13:191–200.

[53] Antoun A, Pavlov MY, Tenson T, Ehrenberg MM. Ribosome formation from subunits studied by stopped-flow and Rayleigh light scattering. Biol Proceed Online 2004;6:35–54.

[54] Kelmers AD, Hancher CW, Phares EF, David Novelli G. Large-scale fermentation of *Escherichia coli* and recovery of transfer ribonucleic acids. Methods Enzymol 1971;20: 3–9.

[55] Pavlov MY, Ehrenberg M. Rate of translation of natural mRNAs in an optimized *in vitro* system. Arch Biochem Biophys 1996;328:9–16.